Monitoring pH-Triggered Drug Release from Radioluminescent Nanocapsules with X-ray Excited Optical Luminescence

Hongyu Chen,[†,¶] Thomas Moore,[‡,¶] Bin Qi,[§] Daniel C. Colvin,[⊥] Erika K. Jelen,[‡] Dale A. Hitchcock,[∥] Jian He,[∥] O. Thompson Mefford,[§] John C. Gore,[⊥] Frank Alexis,[‡,*] and Jeffrey N. Anker[†,*]

[†]Department of Chemistry, Center for Optical Materials Science and Engineering Technology (COMSET), and Environmental Toxicology Program, [‡]Department of Bioengineering, and [§]Department of Materials Science Engineering, Clemson University, Clemson, South Carolina 29634, United States, [⊥]Institute of Imaging Science (VUIIS), Department of Radiology and Radiological Sciences, Vanderbilt University, Nashville, Tennessee 37232, United States, and [∥]Department of Physics & Astronomy, Clemson University, Clemson, South Carolina 29634, United States. [¶]These authors contributed equally to this work.

ABSTRACT One of the greatest challenges in cancer therapy is to develop methods to deliver chemotherapy agents to tumor cells while reducing systemic toxicity to noncancerous cells. A promising approach to localizing drug release is to employ drug-loaded nanoparticles with coatings that release the drugs only in the presence of specific triggers found in the target cells such as pH, enzymes, or light. However, many parameters affect the nanoparticle distribution and drug release rate, and it is difficult to quantify drug release *in situ*. In this work, we show proof-of-principle for a "smart" radioluminescent nanocapsule with an X-ray excited optical luminescence (XEOL) spectrum that changes during release of the optically absorbing chemotherapy drug, doxorubicin. XEOL provides an almost background-free luminescent signal for measuring drug release from particles irradiated by a narrow X-ray beam. We study *in vitro* pH-triggered release rates of doxorubicin from nanocapsules coated with a pH-responsive polyelectrolyte multilayer using HPLC and XEOL spectroscopy. The doxorubicin was loaded to over 5% by weight and released from the capsule with a time constant *in vitro* of ~36 days at pH 7.4 and 21 h at pH 5.0, respectively. The Gd_2O_2S:Eu nanocapsules are also paramagnetic at room temperature with similar magnetic susceptibility and similarly good MRI T_2 relaxivities to Gd_2O_3, but the sulfur increases the radioluminescence intensity and shifts the spectrum. Empty nanocapsules did not affect cell viability up to concentrations of at least 250 μg/mL. These empty nanocapsules accumulated in a mouse liver and spleen following tail vein injection and could be observed *in vivo* using XEOL. The particles are synthesized with a versatile template synthesis technique which allows for control of particle size and shape. The XEOL analysis technique opens the door to noninvasive quantification of drug release as a function of nanoparticle size, shape, surface chemistry, and tissue type.

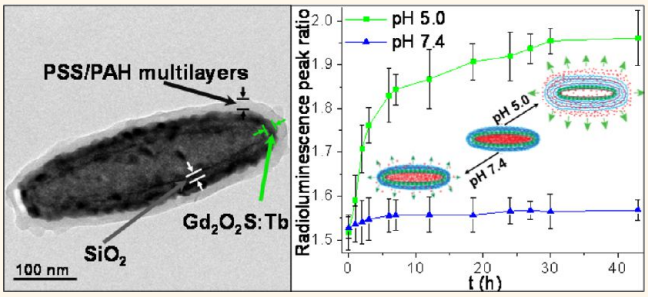

KEYWORDS: pH-triggered drug release · release monitoring · radioluminescent nanocapsules · theranostics

Nanoparticle drug carriers with stimuli-responsive controlled drug release have the potential for site-selective controlled release. Stimuli such as pH,[1−4] temperature,[5,6] redox reactions,[7,8] enzyme,[9−11] and light[12−14] have been studied as triggers for drug release. The *in vivo* drug release rate and location depend upon many factors, including nanoparticle size, shape, composition, and surface chemistry as well as physiological factors such as vasculature and blood flow rate, pH, and enzyme concentration. In principle, one would like to optimize the nanoparticle parameters in order to maximize drug release into tumors and minimize systemic release in the blood; however, it is a challenge to measure release *in vivo* after systemic administration. To rationally design effective chemotherapy carriers, there is a critical need to develop flexible theranostic nanocarriers that can be localized in tissues to monitor drug release at high resolution. While positron emission tomography

* Address correspondence to falexis@clemson.edu; janker@clemson.edu.

Received for review September 20, 2012 and accepted January 2, 2013.

Published online January 02, 2013
10.1021/nn304369m

(PET)[15−17] and single photon emission computed tomography (SPECT)[18] are the most common molecular *in vivo* imaging techniques, there is no way to distinguish encapsulated from released drug.

Doxorubicin (DOX) is a chemotherapy drug used to treat a wide range of cancers. However, its serious adverse effects such as suppression of hemaropoiesis and gastrointestinal and cardiac toxicity limit its applications.[19,20] It is crucial to control the concentration of doxorubicin specifically in the blood circulation, normal tissues, and tumor tissues. Unfortunately, DOX clears rapidly from circulation (circulation half-life of <5 min),[21] which makes it difficult to specifically target tumor cells using free drug. A pH-responsive controlled release system for DOX could address this issue by releasing drugs into the blood only gradually, but rapidly release drugs after endocytosis in acidic tumor lysosomes and endosomes. The particles could be targeted to tumors *via* enhanced permeability and retention (EPR) effect and by functionalizing the nanoparticle surface with appropriate antibodies or other targeting molecules. For example, in 2005, Lee *et al.* reported pH-sensitive micelles as carriers for DOX to enhanced tumor specificity and endosome disruption property on the carrier.[22,23] Recently, mesoporous silica has also gained attention as drug storage and release hosts due to their mesoporous structure, high surface area, and easily modified surface.[24−27] Zhu and co-workers reported pH-controlled delivery of DOX to cancer cells based on small mesoporous carbon nanospheres. However, these studies did not use radioluminescent nanoparticles or provide a method to quantify the release rate *in situ*.

Recently, the Xing group developed X-ray luminescence computed tomography (XLCT) to image the location of radioluminescent particles embedded in tissue using a narrow X-ray beam (*e.g.*, 1 mm) to irradiate the particles and a photodetector to collect the luminescence.[28−32] The X-ray excited optical luminescence is only generated in the path of the narrow X-ray beam which penetrates deeply through tissue and maintains focus through several centimeters. The spatial resolution is determined by the narrow X-ray beam width. The image is formed point-by-point by measuring the total luminescence intensity collected at each X-ray beam position, while the beam is scanned across the sample. A three-dimensional image is generated by rotating the sample relative to the X-ray beam and using tomographic reconstruction algorithms. XLCT is a low-background technique because only the radioluminescent particles emit light during the imaging process. The Xing group also developed a limited-angle X-ray luminescence tomography (XLT) to more rapidly acquire images without rotating the X-ray relative to the sample, but with worse resolution along one of the three dimensions.[33] On the basis of their simulation, this technique allows imaging microgram/milliliter particle concentrations through 5 cm of tissue with ∼10 mGy dose of X-ray. This technique is expected to be especially useful in surgical applications because of its short acquisition time, high depth resolution, and low X-ray dose.

In our previous work, we extended these X-ray excited optical luminescence (XEOL) approaches to perform high spatial resolution chemical analysis in tissue by using the radioluminescent particles as an *in situ* localized light source for spectrochemical analysis in conjunction with nearby chemical indicator dyes. For example, to measure pH on an implanted surface, we placed pH paper upon a radioluminescent film with embedded Gd_2O_2S:Tb particles to alter the their spectral ratio of radioluminescence peaks in a pH-dependent manner.[34] We also demonstrated submillimeter imaging through 1 cm of chicken breast.[34,35] In addition to pH indicators, the principle applies to other materials that absorb light, including silver and gold nanoparticles deposited on films.[36] We also found that the XEOL spectrum of hollow Gd_2O_3:Eu nanoparticles is greatly reduced by the presence of an iron oxide core.[37] Upon the basis of these results, we hypothesized that we could use radioluminescence to monitor the release of dyes and optically absorbing drugs from the core of radioluminescent nanocapsules.

In this work, we synthesize rare-earth (Tb, Eu)-doped Gd_2O_2S-based radioluminescent capsules as a drug nanocarrier and drug release monitor. Compared with gadolinium oxide doped with Eu, Tb- and Eu-doped gadolinium oxysulfide possesses higher photoconversion efficiency (approximately 60 000 visible photons/MeV for Gd_2O_2S:Tb and Gd_2O_2S:Eu, 40 000 visible photons/MeV for Gd_2O_3:Eu).[35] Their bright radioluminescence (see Supporting Information Figure S1) can be used to track the delivered drug and monitor the drug release process. Meanwhile, these capsules serve as good T_2-weighted MRI contrast agents which can be used as a complementary imaging mode for X-ray functional imaging.[35]

RESULTS AND DISCUSSION

Particle shape plays a crucial role in the application of drug delivery systems.[38,39] Some previous studies on particles with high aspect ratio (*e.g.*, nanorod, nanorice) showed that those particles (>500 nm in length) with high aspect ratio have a slower clearance rate than particles with low aspect ratio (*e.g.*, spherical particles) in the application of drug delivery systems.[40,41] We chose ellipsoidal hollow silica nanorice as templates to synthesize monodispersed ellipsoidal nanocapsules. The technique is highly flexible for controlling the nanocapsule size and shape: by varying the synthesis condition of the template,[42−44] the length of these nanocapsules can be tuned from 20 to 600 nm and the aspect ratio can be adjusted from spheres to prolate spheroids. In order to obtain monodispersed silica nanoshells, as

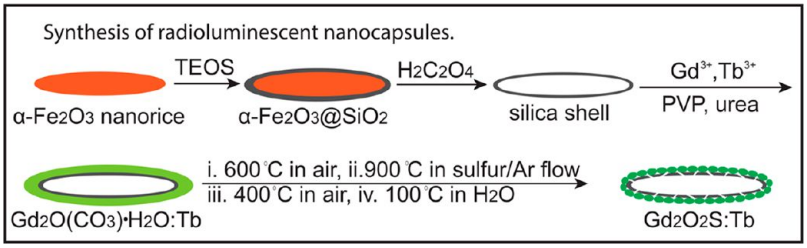

Figure 1. Schematic illustration of the synthesis of radioluminescent nanocapsules.

shown in Figure 1, monodispersed hematite nanorice is first prepared, then treated through a modified Stöber procedure to form a thin silica shell. Finally, the hematite core was removed by etching in 0.5 M oxalic acid for 17 h. The monodispersed silica shell was then coated with a layer of $Gd_2O(CO_3)_2 \cdot H_2O$ doped with terbium (Tb^{3+}/Gd^{3+} = 2.4 mol %) or europium (Eu^{3+}/Gd^{3+} = 5.1 mol %) through a homogeneous precipitation method from gadolinium, europium nitrate. After heat treatment at 600 °C for 1 h, the amorphous $Gd_2O(CO_3)_2 \cdot H_2O$ layer transformed into Gd_2O_3. The above product was treated by sulfur gas with argon flow at 900 °C for 1 h to convert the Gd_2O_3 to Gd_2O_2S. The obtained nanoparticles were reheated at 400 °C in the air for 1 h and incubated in boiling water for 2 h to remove the residue of sulfur and gadolinium sulfide.

TEM images in Figure 2A show monodispersed spindle-shaped iron oxide seeds. Figure 2B represents the intact silica shell after the iron oxide core was removed by dissolving in oxalic acid. The SEM image in Figure 2C and narrow size distribution in Figure 2D indicate that the monondispersed nanocapsules were obtained successfully with an average length of 420 ± 20 nm and width of 130 ± 15 nm. The nanocapsules possess a 10 nm thick inner silica shell and a 25 nm thick outer Gd_2O_2S:Tb radioluminescent shell (Figure 2F) with porous morphology (Figure 2E,G and Supporting Information Figure S2). The pores are irregular in shape, with an average diameter of 8.5 ± 2 nm. These visible pores in the shell (Gd_2O_2S:Tb) of the nanocapsules likely facilitate drug loading and releasing. Crystal structure and composition of these nanocapsules were characterized by powder X-ray diffraction (XRD), and the host is shown as a hexagonal phase of Gd_2O_2S according to the data of JCPDS card no. 26-1422 (Supporting Information Figure S3). Gd_2O_2S:Eu with similar aspect ratio was also synthesized by the same silica nanotemplate (Supporting Information Figures S4 and S5). The tunable size range and the morphology make these nanocapsules promising as drug carriers. In order to apply these nanocapsules in biological applications, the stability of the nanocapsules was tested in 0.3% (vol %) acetic acid (pH ~3.0). The SEM images in Figure S6 show no discernible dissolution, indicating that the nanocapsules are very stable under pH 3 at 37 °C even after 24 h. The cell viability of our X-ray phosphors on MCF-7 breast cancer cells was also tested, and it is shown that cell viability was greater than 90% when the concentration of Gd_2O_2S:Tb and Gd_2O_2S:Eu is as high as 250 μg/mL, after incubation for 24 h (Supporting Information Figure S7).

The radioluminescence spectra of nanocapsules (Gd_2O_2S:Tb, Eu) are presented in Figure 3. The radioluminescence mechanism involves the generation of electron−hole pairs in the host lattice following X-ray absorption. These electron−hole pairs then excite Tb^{3+} and Eu^{3+} centers, which emit visible and near-infrared light. The conversion efficiency is 60 000−70 000 visible photons/MeV X-ray photon in bulk Gd_2O_2S:Eu, corresponding to an energy efficiency of approximately 15%.[45−47] The narrow luminescent peaks of Gd_2O_2S:Tb are attributed to the transitions from the $^5D_4$ excited state to the ^7F_J (J = 6, 5, 4, 3, 2, 1, 0) ground states of the Tb^{3+} ion. The $^5D_4 \rightarrow {}^7F_5$ transition at 544 nm is the most prominent group. The $^5D_{0,1} \rightarrow {}^7F_J$ (J = 0, 1, 2, 4) transition lines of the Eu^{3+} ions generate the intense peak at 590, 612, 620, and 720 nm. The strongest red emission which splits into two peaks at 621 and 612 nm arises from the forced electric dipole $^5D_0 \rightarrow {}^7F_2$ transitions of the Eu^{3+} ions. These nanocapsules displayed similar fluorescence spectra under blue excitation light (460−495 nm) (Supporting Information Figure S8). However, blue light does not penetrate as deeply into tissue as X-rays and, unlike X-rays, does not stay collimated or focused, which dramatically reduces image resolution.

Poly(styrenesulfonate sodium) (PSS) and poly(allylamine hydrochloride) (PAH) are widely used polyelectrolytes in pH-controlled release systems.[1−4] In order to create a stimuli-responsive system for DOX, our X-ray luminescent nanocapsules were coated with eight layers of negatively charged PSS and seven layers of positively charged PAH to encapsulate DOX with layer-by-layer assembly (Figure 4; the particle is denoted as DOX@Gd_2O_2S:Tb@PSS/PAH). Because the surfaces of our nanocapsules are positively charged (+14.9 mV, Figure S9, Supporting Information), the first layer of polyelectrolyte coated on nanocapsules is PSS. After the layer-by-layer coating, the nanocapsules are coated by an average of 30 nm thick polyelectrolyte with a layer of PSS on the surface. Cell viability tests indicate that the empty Gd_2O_2S:Tb nanocapsules coated with PSS/PAH multilayers show no significant toxicity to a concentration of at least 250 μg/mL, the highest concentration

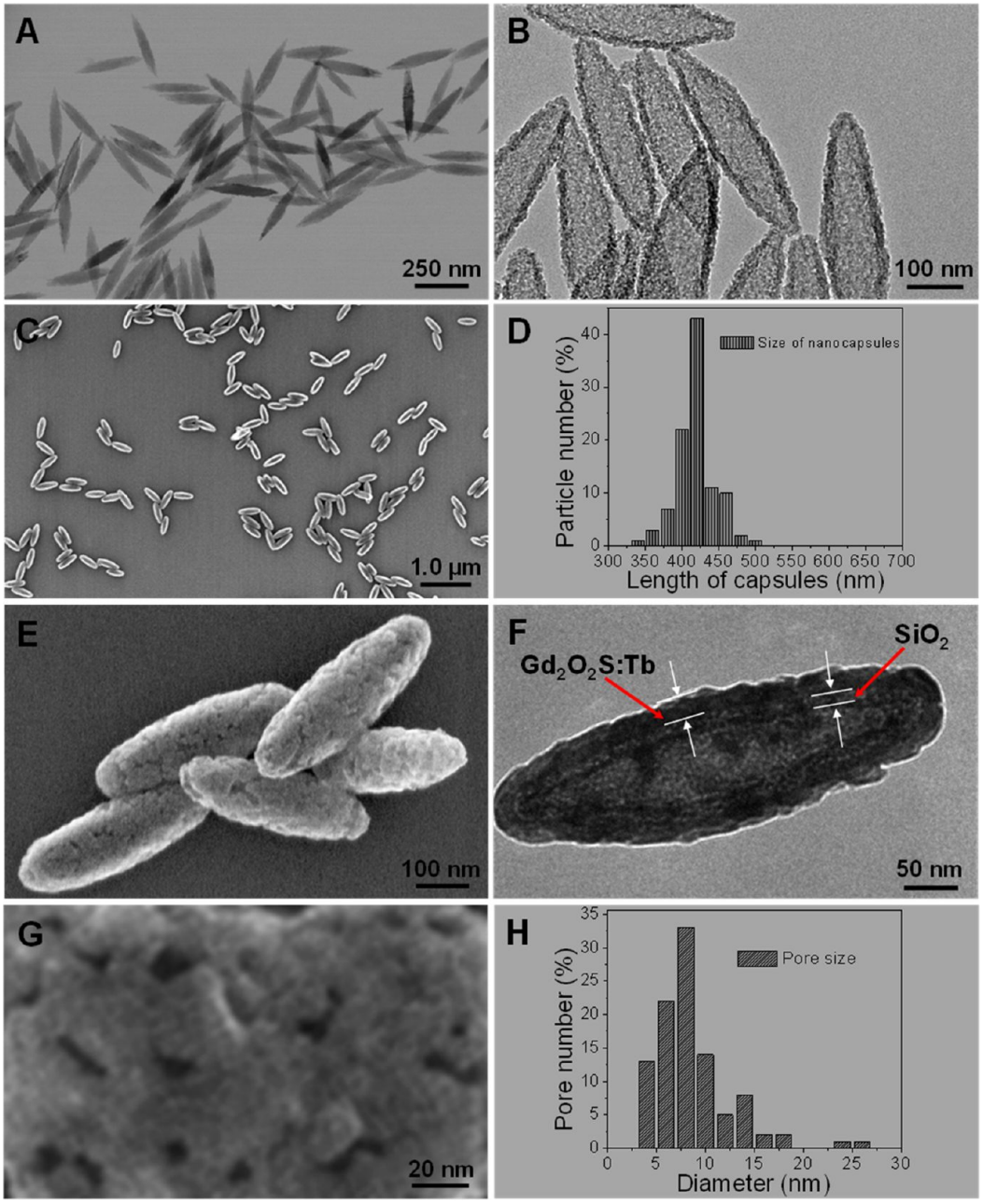

Figure 2. (A) TEM image of monodispersed iron oxide seeds. (B) TEM image of hollow silica shell after removing iron oxide core. (C) SEM image of monodispersed radioluminescent nanocapsule (Gd_2O_2S:Tb (Tb/Gd = 2.4 mol %)). (D) Size distribution of the nanocapsules. (E) High-magnification SEM image of the nanocapsule. (F) TEM image of the nanocapsule. (G) High-magnification SEM image of surface of a nanocapsule. (H) Pore size distribution from 100 nanocapsules with 3786 pores; the diameter of each pore is calculated by the average value of the maximum and minimum length of the pore.

measured (Supporting Information Figure S7). In order to demonstrate that the DOX is loaded into the nanocapsules, nanocapsules filled with a solid core were synthesized as a control by using the silica-coated hematite instead of hollow silica shells as the template. The same DOX loading and polyelectrolyte coating were employed to the nanocapsules with a solid core (iron sulfide). From the released DOX from these solid particles, we calculate that the hollow particles release approximately 20 times more DOX than the solid-core particles, indicating that most of the DOX is stored in the core of the hollow particles (Supporting Information Figure S10).

To study the release rate at normal physiological pH and in acidic cancer environments, we measured the release rate in pH 7.4 PBS and 5.0, respectively. The cumulative release profile of doxorubicin from these nanocapsules is pH-dependent (Figure 5). The drug release is enhanced at pH 5.0, which is applicable for cancer therapy due to the low pH environment in tumors and within endosomes after internalization by cancer cells.[48,49] Upon the basis of exponential fitting

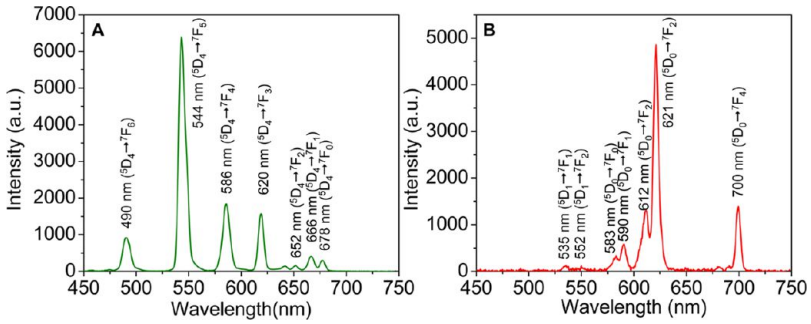

Figure 3. X-ray excited optical luminescence spectra of empty nanocapsules: (A) Gd_2O_2S:Tb, (B) Gd_2O_2S:Eu.

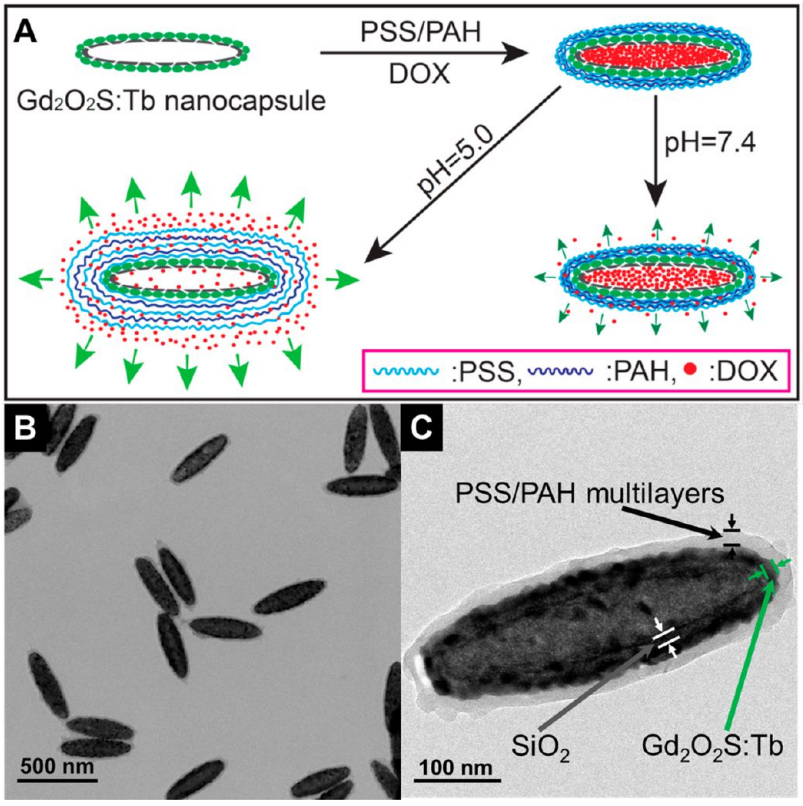

Figure 4. (A) Schematic illustration of the synthesis of DOX@Gd_2O_2S:Tb@PSS/PAH and pH-responsive release of DOX. (B) TEM image of DOX@Gd_2O_2S:Tb@PSS/PAH nanocapsules. (C) High-resolution TEM image of a single DOX@Gd_2O_2S:Tb@PSS/PAH nanocapsule.

to the HPLC release curve, the release rate time constant was estimated to be ~36 days at pH 7.4 and 21 h at pH 5.0. From the released DOX at pH 5.0 after 48 h, the encapsulated DOX in DOX@Gd_2O_2S:Tb@PSS/PAH was over 5% by weight.

Our pH-responsive controlled release system is also able to monitor the release process of DOX at different pH by detecting the radioluminescence of Gd_2O_2S:Tb nanocapsules (Figure 6). The radioluminescence peak ratio is shown to be very sensitive to the early release of DOX, especially in the first 10 h. The single exponential fit time constant for the radioluminescence peak ratio was estimated to be 4 h at pH 5.0, and ~ 7 days at pH 7.4. At pH 5.0 and 7.4, DOX has a similar broad absorption of light from 350 to 600 nm, which overlaps with some of the XEOL peaks of Gd_2O_2S:Tb (Figure 6A). Figure 6B shows that the intensity ratio of X-ray luminescence at 544 and 620 nm increases with the release of doxorubicin because local luminescence absorption by DOX decreases when DOX is released. We observed the similar luminescent increase of nanoparticle with iron oxide as a core when the iron oxide is partially dissolved.[37] The mechanism is likely a combination of near-field absorption and/or energy transfer. Future work will elucidate the mechanism by measuring the XEOL spectra and lifetime. The peak intensity ratio reaches a maximum value when the DOX concentration in the particles is in equilibrium with the solution concentration.

In order to examine the uptake of these nanocapsules by cancer cells, nanocapsules doped with europium (Gd_2O_2S:Eu) were incubated with MCF-7 cancer cell and washed multiple times to eliminate nanocapsules

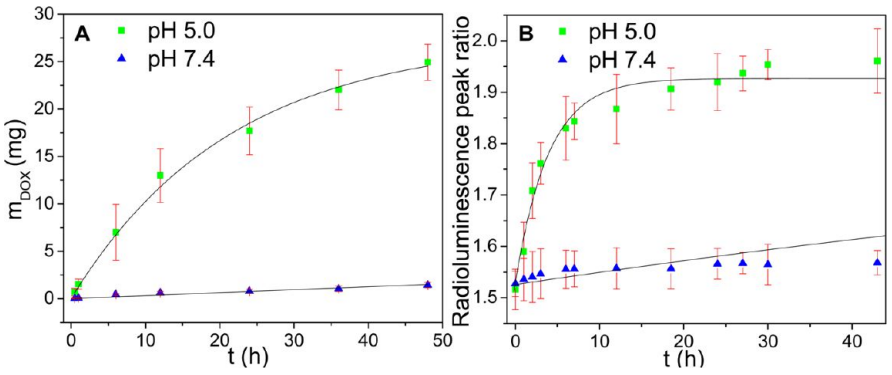

Figure 5. (A) Cumulative release of doxorubicin from DOX@Gd_2O_2S:Tb@PSS/PAH at pH 5.0 and 7.4, measured with HPLC. The line fits data to a single exponential curve with a saturation of 27.4 mg. This saturation is calculated based on the fit at pH 5.0. (B) Peak ratio of real time radioluminescence intensity at 544 and 620 nm as a function time in pH 5.0 and 7.4 buffers. The line fits data to a single exponential curve with a saturation ratio of 1.93. This saturation is calculated based on the fit at pH 5.0.

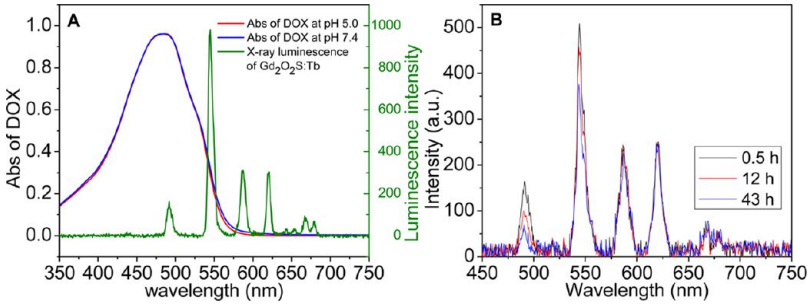

Figure 6. (A) Absorption spectra of DOX (0.05 mg/mL at pH 5.0 and 7.4) and radioluminescence spectrum of Gd_2O_2S:Tb@PSS/PAH. (B) Radioluminescent spectra of DOX@Gd_2O_2S:Tb@PSS/PAH at pH 5.0 taken at three different times during drug release.

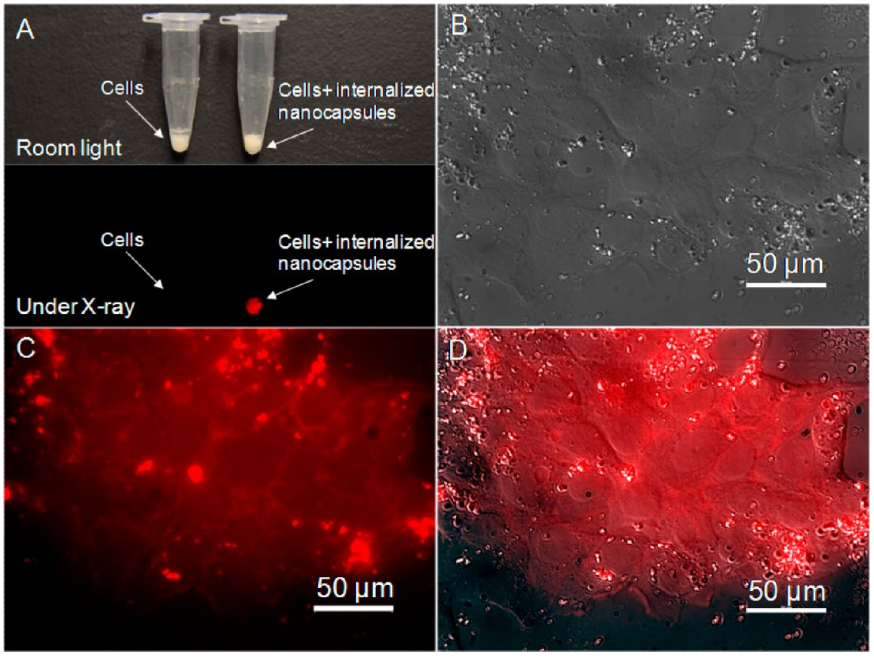

Figure 7. (A) Photograph of MCF-7 breast cancer cells with and without internalized nanocapsules (Gd_2O_2S:Eu) viewed under room light and X-ray irradiation. (B) Transmitted light differential interference contrast microscopy image of MCF-7 cells with internalized nanocapsules (Gd_2O_2S:Eu). Fluorescence microscopy image of the cells shown in (B). (D) Merged image of (B) and (C).

from the cell culture media. The internalized nanocapsules were brightly luminescent under X-ray radiation (Figure 7A). The bright fluorescence signal of nanocapsules is very useful in drug localization and cell labeling. Figure 7C shows the fluorescence signal of the Gd_2O_2S:Eu nanocapsules in MCF-7 cancer cells after multiple washing steps to eliminate nanocapsules from the cell culture media.

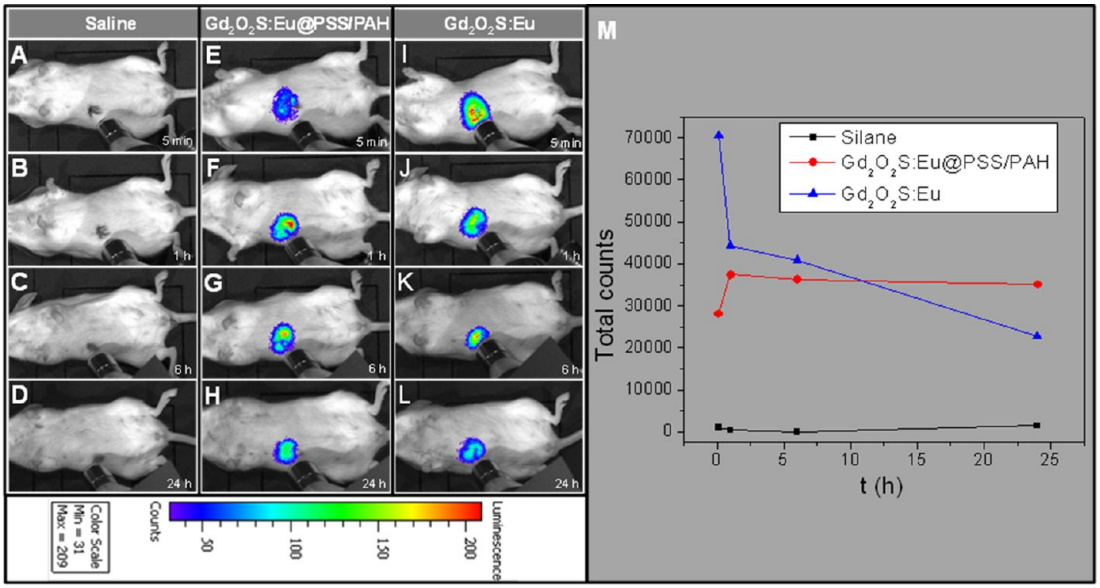

Figure 8. Representative luminescent images of accumulation of Gd_2O_2S:Eu nanocapsules with and without polymer coating in a mouse model, with the X-ray beam irradiating the liver. (A) 5 min, (B) 1 h, (C) 6 h, (D) 24 h after the mouse was injected with saline (200 μL). (E) 5 min, (F) 1 h, (G) 6 h, (H) 24 h after the mouse was injected with Gd_2O_2S:Eu@PAH/PSS nanocapsules (200 μL, 1 mg/mL). (I) 5 min, (J) 1 h, (K) 6 h, (L) 24 h after the mouse was injected with Gd_2O_2S:Eu nanocapsules (200 μL, 1 mg/mL). (M) Total radioluminescence intensity counts as a function of time after injection.

To demonstrate that the nanoparticle XEOL can be imaged *in vivo* using a IVIS Lumina-XR imaging system (Caliper Life Sciences, Hopkinton, MA, USA) during irradiation with a miniature X-ray source (Amptek mini X-ray tube, Ag target, Amptek Inc. MA, USA), 200 μL of 1 mg/mL Gd_2O_2S:Eu nanocapsules coated with PSS/PAH multilayers was injected into a mouse tail vein. The effective nanocapsule concentration in the mouse is about 133 μg/mL (the blood volume of a mouse is around 1.5 mL), which did not affect cell viability for MCF-7 breast cancer cells *in vitro*. Furthermore, a preliminary maximum tolerated dose (MTD) study was carried out, and it shows that no morbidity or weight loss was observed for doses up to 400 mg/kg. The *in vivo* accumulation of the nanocapsules in the liver was evident under X-ray irradiation with 0.1 s exposure time. Compared to the Gd_2O_2S:Eu without PSS/PAH multilayers (Figure 8), the accumulation rate for polyelectrolyte-coated nanocapsules is slower in the first 1 h. Post mortem, XEOL images of the excised organs confirmed that the nanocapsules accumulated in liver and spleen (Supporting Information Figure S11).

Recent studies describe the synthesis and applications of gadolinium oxide (Gd_2O_3) nanoparticles as MRI contrast agents.[37,50−54] However, to our knowledge, no investigation of gadolinium oxysulfide (Gd_2O_2S)-based MRI contrast agents has been reported so far. Our luminescent nanocapsules mainly consisting of Gd_2O_2S also have similar magnetic properties to gadolinium oxide, which make them a potential MRI contrast agent.[37] Room temperature magnetic hysteresis loops of the nanocapsules (Gd_2O_2S:Tb, Gd_2O_2S:Eu) are shown in Figure S12. Both types of

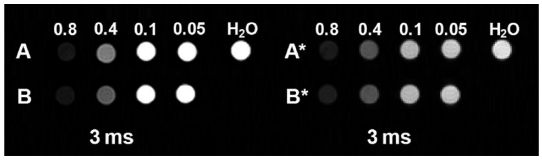

Figure 9. T_2- and T_2*-weighted images of radioluminescent nanocapsules. Group A: T_2-weighted images of Gd_2O_2S:Eu nanocapsules with concentration of 0.8, 0.4, 0.1, and 0.05 mg/mL. Group B: T_2-weighted images of Gd_2O_2S:Tb with concentration of 0.8, 0.4, 0.1, and 0.05 mg/mL. Group A*: T_2*-weighted images of Gd_2O_2S:Eu nanocapsules with concentration of 0.8, 0.4, 0.1, and 0.05 mg/mL. Group B*: T_2*-weighted images of Gd_2O_2S:Tb nanocapsules with concentration of 0.8, 0.4, 0.1, and 0.05 mg/mL.

nanocapsules are paramagnetic, as evident by the linear relation between the particle magnetization and the applied magnetic field with no indication of saturation up to applied fields of at least 30 kOe. Both Gd_2O_2S:Tb and Gd_2O_2S:Eu nanocapsules had almost identical magnetic susceptibilities of 1.2×10^{-4} emu g^{-1} Oe^{-1}.

We performed *in vitro* MR assays (T_2- and T_2*-weighted imaging) in 0.5% agarose gel for both types of Gd_2O_2S:Tb and Gd_2O_2S:Eu nanocapsules with a series of concentration (0.8, 0.4, 0.1, and 0.05 mg/mL). Figure 9 shows T_2- and T_2*-weighted images after 3 ms. The proton relaxivities, r_2, of the nanocapsules were determined from the transverse relaxation rates at various concentrations. These relaxation rates are shown as a function of concentration in Figure S13. The relaxivities r_2 and r_2* are 50.3 and 116.0 mM^{-1} s^{-1}, respectively, for Gd_2O_2S:Tb nanocapsules and 51.7 and 116.4 mM^{-1} s^{-1} for Gd_2O_2S:Eu nanocapsules.

For these nanocapsules, r_2* is larger than r_2 due to the inhomogeneities of local static field from the mag-

netic moment of the particles. Previous work on gadolinium oxide nanoparticles (*e.g.*, ultrasmall Gd_2O_3 nanoparticles (1−10 nm)[50−53] and hollow nanosparticles with thin Gd_2O_3 shell (∼10 nm)[54]) reported that they can served as good T_1 contrast agents and moderate T_2 contrast agents. However, our nanocapsules with a ∼25 nm Gd_2O_2S-based nanoshell worked as a better T_2 contrast agent than many reported Gd_2O_3 nanoparticles (r_2 = 14.1−16.9 mM^{-1} s^{-1})[55−57] and gadolinium chelates (Gd-DOTA, 4.9 mM^{-1} s^{-1}).[55] In addition, the T_2 relaxivity value of our nanocapsules is similar to FDA-approved iron oxide nanoparticle contrast agents such as Ferumoxtran (Resovist, 65 mM^{-1} s^{-1}), cross-linked iron oxide particles (CLIO-Tat, 62 mM^{-1} s^{-1}), and water-soluble iron oxide (WSIO, 78 mM^{-1} s^{-1}).[58−61]

CONCLUSION

In summary, we present a flexible template-directed method to produce radioluminescent nanocapsules to carry hydrophilic drugs and monitor release kinetics. The release rate time constant was ∼36 days at pH 7.4 and 21 h at pH 5.0. Importantly, the release mechanisms could be monitored *in situ* by tracking the ratio of radioluminescence spectral peaks. Radioluminescence offers several advantages over traditional optical imaging agents, including greater tissue penetration, elimination of autofluorescence, and the ability to perform high-resolution imaging through thick tissue *via* functional X-ray luminescence tomography (FXLT).[30,32,34,36] Finally, the multifunctional nanocapsules combined the advantages of positive contrast of radioluminescence and negative contrast of T_2-weighted MR imaging. These capabilities allow these nanocapsules to enable novel drug delivery and imaging modalities. In the future, we plan to target DOX-loaded capsules to tumors and measure *in situ* release rates and tumor growth for various nanocapsule sizes, shapes, and surface chemistries.

EXPERIMENTAL SECTION

Materials. Tetraethoxysilane (TEOS), poly(styrenesulfonate sodium) (PSS, MW ∼70 000), and iron(III) chloride anhydrous were purchased from Sigma-Aldrich (St. Louis, MO). Gadolinium nitrate, europium nitrate, and poly(allylamine hydrochloride) (PAH, MW ∼15 000) were purchased from Alfa Aesar (Ward Hill, MA). Ethanol (96%), urea, oxalic acid, ammonium hydroxide, and nitric acid were obtained from BDH Chemicals Ltd. (Poole, Dorset, UK). Deionized (DI) water was purchased from EMD Chemicals Inc. (Gibbstown, NJ, USA). Polyvinylpyrrolidone (PVP K-30, MW 40 000) was purchased from Spectrum Chemicals (Gardena, CA). Agarose (melting point 88 ± 1 °C) was purchased from Shelton Scientific (Peosta, IA). All chemicals were used as received without further purification.

Preparation of Nanocapsules Gd_2O_2S:Tb and Gd_2O_2S:Eu. Monodispersed spindle-shaped hematite nanotemplates with controllable aspect ratios were prepared according to the method described by Ozaki and co-workers.[43] Typically, 100 mL of aqueous solution containing 2.0 × 10^{-2} M $FeCl_3$ and 3.6 × 10^{-4} M KH_2PO_4 was aged at 100 °C for 72 h. The resulting precipitate was centrifuged and washed three times with water. The hollow silica shell was obtained according to the literature.[37,62,63] The spindle-shaped hematite particles synthesized above were dispersed ultrasonically to a 80 mL solution containing PVP (0.6 g), water (6 mL), and ethanol (74 mL). The suspension was stirred using a magnetic stir bar at room temperature, and a solution of TEOS (270 μL) in 20 mL of ethanol was added, followed by 4 mL of ammonia hydroxide. After 3 h, the reaction mixture was precipitated by centrifuging at 4000 rpm for 16 min. The particles were washed three times with ethanol and centrifuged to collect the product. These silica-coated hematite nanoparticles were then suspended in 180 mL of distilled water with 1.8 g of PVP and 11.34 g of oxalic acid dihydrate and incubated at 60 °C for 17 h in order to dissolve the hematite core. The silica shell particles were collected by centrifugation and rinsed with DI water twice. The obtained hollow nanoshells were resuspended with 3 mL of $Gd(NO_3)_3$ (1 M), 0.94 mL of $Tb(NO_3)_3$ (80 mM), or 1.5 mL of $Eu(NO_3)_3$ (80 mM), and 1.8 g of PVP in DI water to form 300 mL of solution. Eighteen grams of urea was added to the solution, and the solution was maintained at 80 °C for 60 min. The precursor of radioluminescent nanocapsules was collected by centrifugation and calcined in a furnace at 600 °C for 60 min. The powder was then transferred to a tube furnace with a sulfur/argon flow at 900 °C for 60 min. The obtained nanocapsules were reheated at 400 °C in the air for 1 h and incubated in distilled water (2.5 mg/mL) at 100 °C for 2 h prior to use.

Preparation of Polyelectrolyte Multilayer Coating. Two milliliters of PSS with a concentration of 5 mg mL^{-1} in 0.5 M NaCl solution was added slowly (drop by drop) to a 10 mL aqueous suspension (pH 6) of 50 mg of DOX and 30 mg of nanocapsules (Gd_2O_2S:Tb). After ultrasonic treatment for 10 min, the suspension was collected by centrifugation and washed three times in distilled water. Gentle shaking followed by ultrasonic treatment for 1 min was used to disperse the particles in 10 mL distilled water. Then, 2 mL oppositely charged PAH (5 mg/mL in 0.5 M NaCl) with 50 mg DOX was added slowly to the nanocapsule solution and the solution was sonicated for 10 min. The PSS coating process was repeated eight times, and the PAH coating was repeated seven times. Finally, a composite of DOX−nanocapsules coated with PAH/PSS multilayers was obtained.

***In Vitro* HPLC Drug Release Study.** One hundred microliters of DOX-encapsulated nanocapsules with polyelectrolyte multilayers (10 mg/mL) was suspended with release media (7 mL) at pH 5.0 and 7.4 in Slide-A-Lyzer MINI dialysis units at room temperature. The release medium was removed for analysis at given time intervals and replaced with the same volume of fresh release medium. The DOX concentration was measured with high-performance liquid chromatography (HPLC) on a Waters system using an Alltima C18 column (250 × 4.6 mm, 5 μm).

Radioluminescence Drug Release Tracking Experiment. Two milliliters of DOX-encapsulated nanocapsules with polyelectrolyte multilayers (25 mg/mL) was magnetically stirred at a rate of 400 rpm in release media of either pH 5 or 7.4. Fifty microliters of the solution was taken out for X-ray luminescence analysis without any separation at given time intervals.

Preparation of Nanocapsules for MR Imaging. T_2 and T_2* MR measurements were acquired for the spindle-shaped SiO_2@Gd_2O_2S:Eu and Gd_2O_2S:Tb particles at a series of concentrations (0.8, 0.4, 0.1, and 0.05 mg/mL). The particles were dispersed in 0.5% agarose gel at 80 °C and cooled to room temperature in NRM tubes to set the gel. The gel prevented settling and aggregation, allowing MR imaging several days after preparation.

Cell Viability Test. MCF-7 breast cancer cells were seeded at a density of 10 000 cells/well in a 96-well plate. Cells were stored at 37 °C at 5% CO_2 and attached to the plate overnight. Nanocapsules were suspended in media, sonicated for 10 min to disperse, and diluted to 250, 100, 50, and 10 μg/mL. Medium was removed from the wells, and fresh medium or nanoparticle in media was added to each well. Five repeats were done for each concentration. Nanoparticles were incubated with cells

overnight, and the next day a Presto Blue assay (Life Technologies) was performed. Medium was removed, and 100 μL of a 1:9 ratio Presto Blue in culture media was added to each well. Cells were incubated at 37 °C and 5% CO_2 for 45 min. Fluorescence intensity was taken with a plate reader with an excitation wavelength of 560 nm and an emission wavelength of 590 nm. Fluorescence intensity for each concentration of nanoparticle was normalized as a percentage of the fluorescence intensity of the control cells. Percent viability averages were plotted with error bars of one standard deviation.

Characterization Methods. Transmission and scanning electron microscopy (TEM) were performed on a H9500 operated at 200 kV and HD2000 microscope operated at 20 kV, respectively. Powder XRD patterns were obtained on a Rigaku diffractometer at 40 kV and 40 mA (Cu Kα radiation). For fluorescence spectra, 480 nm light was used to excite the scintillators. To measure radioluminescence, X-ray was generated by a mini X-ray tube (Amptek Inc. MA, USA), and the X-ray tube was operated with a tube voltage of 40 kV and a tube current of 99 μA. The sample was mounted on a Leica microscope (Leica DMI 5000M, Wetzlar, Germany) equipped with a DeltaNu DNS 300 spectrometer (Intevac-DeltaNu, Laramie, WY, USA) with a 150 lines/mm grating blazed at 500 nm and with a cooled CCD camera (iDUS-420BV, Andor, South Windsor, CT, USA). X-ray luminescence images were captured in an IVIS Lumina-XR imaging system (Caliper Life Sciences, Hopkinton, MA, USA) with 0.1 s exposure time. Bright-field and fluorescent images were taken on a Nikon microscope (Eclipse Ti, Nikon, Melville, NY, USA). Determination of the zeta-potential of the nanoparticles was performed *via* a Zetasizer Nano ZS (with a 633 nm He−Ne laser) from Malvern Instrument. Prior to the experiment, the particles were diluted in distilled water (0.1 mg/mL). Magnetization measurements were performed at the designated temperature using the vibrating sample magnetometer (VSM) option of the physical property measurement system (PPMS, Quantum Design, USA), with the applied magnetic field sweeping between $\pm$3.0 T at a rate of 50 Oe/s. Determination of the gadolinium content in a sample was performed by inductively coupled plasma (ICP) (Optima 3100 RL; Perkin-Elmer). All MRI experiments were performed on a Varian 4.7T horizontal bore imaging system (Agilent Inc., Santa Clara, CA). Samples, contained in 5 mm NMR tubes, were placed in a 63 mm inner diameter quadrature RF coil for imaging.

Conflict of Interest: The authors declare no competing financial interest.

Acknowledgment. This research was supported by The Center of Biomaterials for Tissue Regeneration (CBTR) funded under NIH Grants 5P20RR021949 and 8P20GM103444. We thank the Clemson University Electron Microscope Facility for use of TEM imaging facilities. We also thank Professor Shiou-Jyh Hwu for use of his furnace.

Supporting Information Available: Figures to address the characterization in terms of spectroscopy, electron microscopy images, toxicity, magnetic hysteresis, and magnetic resonance relaxivities. This material is available free of charge *via* the Internet at http://pubs.acs.org.

REFERENCES AND NOTES

1. Zhu, Y.; Shi, J.; Shen, W.; Dong, X.; Feng, J.; Ruan, M.; Li, Y. Stimuli-Responsive Controlled Drug Release from a Hollow Mesoporous Silica Sphere/Polyelectrolyte Multilayer Core−Shell Structure. *Angew. Chem., Int. Ed.* **2005**, *44*, 5083–5087.
2. Shchukin, D. G.; Sukhorukov, G. B.; Möhwald, H. Smart Inorganic/Organic Nanocomposite Hollow Microcapsules. *Angew. Chem.* **2003**, *115*, 4610–4613.
3. Sukhorukov, G.; Dähne, L.; Hartmann, J.; Donath, E.; Möhwald, H. Controlled Precipitation of Dyes into Hollow Polyelectrolyte Capsules Based on Colloids and Biocolloids. *Adv. Mater.* **2000**, *12*, 112–115.
4. Ibarz, G.; Dähne, L.; Donath, E.; Möhwald, H. Smart Micro- and Nanocontainers for Storage, Transport, and Release. *Adv. Mater.* **2001**, *13*, 1324–1327.
5. Choi, S.-W.; Zhang, Y.; Xia, Y. A Temperature-Sensitive Drug Release System Based on Phase-Change Materials. *Angew. Chem.* **2010**, *122*, 8076–8080.
6. Jeong, B.; Bae, Y. H.; Kim, S. W. Drug Release from Biodegradable Injectable Thermosensitive Hydrogel of PEG−PLGA−PEG Triblock Copolymers. *J. Controlled Release* **2000**, *63*, 155–163.
7. Li, Y. L.; Zhu, L.; Liu, Z.; Cheng, R.; Meng, F.; Cui, J. H.; Ji, S. J.; Zhong, Z. Reversibly Stabilized Multifunctional Dextran Nanoparticles Efficiently Deliver Doxorubicin into the Nuclei of Cancer Cells. *Angew. Chem., Int. Ed.* **2009**, *48*, 9914–9918.
8. Saito, G.; Swanson, J. A.; Lee, K. D. Drug Delivery Strategy Utilizing Conjugation *via* Reversible Disulfide Linkages: Role and Site of Cellular Reducing Activities. *Adv. Drug Delivery Rev.* **2003**, *55*, 199–215.
9. Wang, C.; Chen, Q.; Wang, Z.; Zhang, X. An Enzyme-Responsive Polymeric Superamphiphile. *Angew. Chem.* **2010**, *122*, 8794–8797.
10. Olson, E. S.; Jiang, T.; Aguilera, T. A.; Nguyen, Q. T.; Ellies, L. G.; Scadeng, M.; Tsien, R. Y. Activatable Cell Penetrating Peptides Linked to Nanoparticles as Dual Probes for *In Vivo* Fluorescence and MR Imaging of Proteases. *Proc. Natl. Acad. Sci. U.S.A.* **2010**, *107*, 4311–4316.
11. Bernardos, A.; Aznar, E.; Marcos, M. D.; Martínez-Máñez, R.; Sancenón, F.; Soto, J.; Barat, J. M.; Amorós, P. Enzyme-Responsive Controlled Release Using Mesoporous Silica Supports Capped with Lactose. *Angew. Chem.* **2009**, *121*, 5998–6001.
12. Skirtach, A. G.; Muñoz Javier, A.; Kreft, O.; Köhler, K.; Piera Alberola, A.; Möhwald, H.; Parak, W. J.; Sukhorukov, G. B. Laser-Induced Release of Encapsulated Materials inside Living Cells. *Angew. Chem.* **2006**, *118*, 4728–4733.
13. You, J.; Zhang, G.; Li, C. Exceptionally High Payload of Doxorubicin in Hollow Gold Nanospheres for Near-Infrared Light-Triggered Drug Release. *ACS Nano* **2010**, *4*, 1033–1041.
14. Wu, G.; Mikhailovsky, A.; Khant, H. A.; Fu, C.; Chiu, W.; Zasadzinski, J. A. Remotely Triggered Liposome Release by Near-Infrared Light Absorption *via* Hollow Gold Nanoshells. *J. Am. Chem. Soc.* **2008**, *130*, 8175–8177.
15. Hong, H.; Zhang, Y.; Sun, J.; Cai, W. Molecular Imaging and Therapy of Cancer with Radiolabeled Nanoparticles. *Nano Today* **2009**, *4*, 399–413.
16. Liu, Z.; Cai, W.; He, L.; Nakayama, N.; Chen, K.; Sun, X.; Chen, X.; Dai, H. *In Vivo* Biodistribution and Highly Efficient Tumour Targeting of Carbon Nanotubes in Mice. *Nat. Nanotechnol.* **2007**, *2*, 47–52.
17. Zhang, F.; Zhu, L.; Liu, G.; Hida, N.; Lu, G.; Eden, H. S.; Niu, G.; Chen, X. Multimodality Imaging of Tumor Response to Doxil. *Theranostics* **2011**, *1*, 302–309.
18. Jaszczak, R. J.; Coleman, R. E.; Whitehead, F. R. Physical Factors Affecting Quantitative Measurements Using Camera-Based Single Photon Emission Computed Tomography (Spect). *IEEE Trans. Nucl. Sci.* **1981**, *28*, 69–80.
19. Morelli, D.; Ménard, S.; Colnaghi, M. I.; Balsari, A. Oral Administration of Anti-Doxorubicin Monoclonal Antibody Prevents Chemotherapy-Induced Gastrointestinal Toxicity in Mice. *Cancer Res.* **1996**, *56*, 2082–2085.
20. Von Hoff, D. D.; Layard, M. W.; Basa, P.; Davis, J. H. L.; Von Hoff, A. L.; Rozencweig, M.; Muggia, F. M. Risk Factors for Doxorubicin-Induced Congestive Heart Failure. *Ann. Intern. Med.* **1979**, *91*, 710–717.
21. Gabizon, A.; Shmeeda, H.; Barenholz, Y. Pharmacokinetics of PEGylated Liposomal Doxorubicin: Review of Animal and Human Studies. *Clin. Pharmacokinet.* **2003**, *42*, 419–436.
22. Lee, E. S.; Na, K.; Bae, Y. H. Doxorubicin Loaded pH-Sensitive Polymeric Micelles for Reversal of Resistant MCF-7 Tumor. *J. Controlled Release* **2005**, *103*, 405–418.
23. Lee, E. S.; Na, K.; Bae, Y. H. Super pH-Sensitive Multifunctional Polymeric Micelle. *Nano Lett.* **2005**, *5*, 325–329.
24. Andersson, J.; Rosenholm, J.; Areva, S.; Lindén, M. Influences of Material Characteristics on Ibuprofen Drug Loading and Release Profiles from Ordered Micro- and Mesoporous Silica Matrices. *Chem. Mater.* **2004**, *16*, 4160–4167.

25. Barbé, C.; Bartlett, J.; Kong, L.; Finnie, K.; Lin, H. Q.; Larkin, M.; Calleja, S.; Bush, A.; Calleja, G. Silica Particles: A Novel Drug Delivery System. *Adv. Mater.* **2004**, *16*, 1959–1966.
26. Lai, C. Y.; Trewyn, B. G.; Jeftinija, D. M.; Jeftinija, K.; Xu, S.; Jeftinija, S.; Victor, S. Y. L. A Mesoporous Silica Nanosphere-Based Carrier System with Chemically Removable CdS Nanoparticle Caps for Stimuli-Responsive Controlled Release of Neurotransmitters and Drug Molecules. *J. Am. Chem. Soc.* **2003**, *125*, 4451–4459.
27. Zhu, Y.; Shi, J.; Shen, W.; Dong, X.; Feng, J.; Ruan, M.; Li, Y. Stimuli-Responsive Controlled Drug Release from a Hollow Mesoporous Silica Sphere/Polyelectrolyte Multilayer Core–Shell Structure. *Angew. Chem.* **2005**, *117*, 5213–5217.
28. Carpenter, C. M.; Sun, C.; Pratx, G.; Liu, H.; Cheng, Z.; Xing, L. Radioluminescent Nanophosphors Enable Multiplexed Small-Animal Imaging. *Opt. Express* **2012**, *20*, 11598–11604.
29. Sun, C.; Pratx, G.; Carpenter, C. M.; Liu, H.; Cheng, Z.; Gambhir, S. S.; Xing, L. Synthesis and Radioluminescence of PEGylated Eu^{3+}-Doped Nanophosphors as Bioimaging Probes. *Adv. Mater.* **2011**, *23*, H195–H199.
30. Pratx, G.; Carpenter, C. M.; Sun, C.; Lei, X. X-ray Luminescence Computed Tomography *via* Selective Excitation: A Feasibility Study. *IEEE Trans. Med. Imaging* **2010**, *29*, 1992–1999.
31. Pratx, G.; Carpenter, C. M.; Sun, C.; Rao, R. P.; Xing, L. Tomographic Molecular Imaging of X-ray-Excitable Nanoparticles. *Opt. Lett.* **2010**, *35*, 3345–3347.
32. Carpenter, C.; Sun, C.; Pratx, G.; Rao, R.; Xing, L. Hybrid X-ray/Optical Luminescence Imaging: Characterization of Experimental Conditions. *Med. Phys.* **2010**, *37*, 4011–4018.
33. Carpenter, C. M.; Pratx, G.; Sun, C.; Xing, L. Limited-Angle X-ray Luminescence Tomography: Methodology and Feasibility Study. *Phys. Med. Biol.* **2011**, *56*, 3487–3502.
34. Chen, H.; Patrick, A. L.; Yang, Z.; VanDerveer, D. G.; Anker, J. N. High-Resolution Chemical Imaging through Tissue with an X-ray Scintillator Sensor. *Anal. Chem.* **2011**, *83*, 5045–5049.
35. Chen, H.; Rogalski, M. M.; Anker, J. N. Advances in Functional X-ray Imaging Techniques and Contrast Agents. *Phys. Chem. Chem. Phys.* **2012**, *14*, 13469–13486.
36. Chen, H.; Longfield, D. E.; Varahagiri, V. S.; Nguyen, K. T.; Patrick, A. L.; Qian, H.; VanDerveer, D. G.; Anker, J. N. Optical Imaging in Tissue with X-ray Excited Luminescent Sensors. *Analyst* **2011**, *136*, 3438–3445.
37. Chen, H.; Colvin, D. C.; Qi, B.; Moore, T.; He, J.; Mefford, O. T.; Alexis, F.; Gore, J. C.; Anker, J. N. Magnetic and Optical Properties of Multifunctional Core–Shell Radioluminescence Nanoparticles. *J. Mater. Chem.* **2012**, *22*, 12802–12809.
38. Decuzzi, P.; Godin, B.; Tanaka, T.; Lee, S. Y.; Chiappini, C.; Liu, X.; Ferrari, M. Size and Shape Effects in the Biodistribution of Intravascularly Injected Particles. *J. Controlled Release* **2010**, *141*, 320–327.
39. Gratton, S. E. A.; Ropp, P. A.; Pohlhaus, P. D.; Luft, J. C.; Madden, V. J.; Napier, M. E.; DeSimone, J. M. The Effect of Particle Design on Cellular Internalization Pathways. *Proc. Natl. Acad. Sci. U.S.A.* **2008**, *105*, 11613–11618.
40. Champion, J. A.; Mitragotri, S. Role of Target Geometry in Phagocytosis. *Proc. Natl. Acad. Sci. U.S.A.* **2006**, *103*, 4930–4934.
41. Huang, X.; Li, L.; Liu, T.; Hao, N.; Liu, H.; Chen, D.; Tang, F. The Shape Effect of Mesoporous Silica Nanoparticles on Biodistribution, Clearance, and Biocompatibility *in Vivo*. *ACS Nano* **2011**, *5*, 5390–5399.
42. Ishikawa, T.; Matijevic, E. Formation of Monodispersed Pure and Coated Spindle-Type Iron Particles. *Langmuir* **1988**, *4*, 26–31.
43. Ozaki, M.; Kratohvil, S.; Matijević, E. Formation of Monodispersed Spindle-Type Hematite Particles. *J. Colloid Interface Sci.* **1984**, *102*, 146–151.
44. Piao, Y.; Kim, J.; Na, H. B.; Kim, D.; Baek, J. S.; Ko, M. K.; Lee, J. H.; Shokouhimehr, M.; Hyeon, T. Wrap-Bake-Peel Process for Nanostructural Transformation from β-FeOOH Nanorods to Biocompatible Iron Oxide Nanocapsules. *Nat. Mater.* **2008**, *7*, 242–247.
45. Franz, K. A.; Kehr, W. G.; Siggel, A.; Wieczoreck, J.; Adam, W. Luminescent Materials. In *Ullmann's Encyclopedia of Industrial Chemistry*; Wiley-VCH: Weinheim, Germany, 2000.
46. Okumura, M.; Tamatani, M.; Matsuda, N.; Takahara, T.; Fukuta, Y. Ceramic Scintillator, Method for Producing Same, and X-ray Detector and X-ray CT Imaging Equipment Using Same. U.S. Patent 6,384,417, 2002.
47. van Eijk, C. W. E. Inorganic Scintillators in Medical Imaging. *Phys. Med. Biol.* **2002**, *47*, R85–R106.
48. Schmaljohann, D. Thermo- and pH-Responsive Polymers in Drug Delivery. *Adv. Drug Delivery Rev.* **2006**, *58*, 1655–1670.
49. Lee, E. S.; Gao, Z.; Bae, Y. H. Recent Progress in Tumor pH Targeting Nanotechnology. *J. Controlled Release* **2008**, *132*, 164–170.
50. Petoral, R. M.; Söderlind, F.; Klasson, A.; Suska, A.; Fortin, M. A.; Abrikossova, N.; Selegård, L. A.; Käll, P.-O.; Engström, M.; Uvdal, K. Synthesis and Characterization of Tb^{3+}-Doped Gd_2O_3 Nanocrystals: A Bifunctional Material with Combined Fluorescent Labeling and MRI Contrast Agent Properties. *J. Phys. Chem. C* **2009**, *113*, 6913–6920.
51. Park, J. Y.; Baek, M. J.; Choi, E. S.; Woo, S.; Kim, J. H.; Kim, T. J.; Jung, J. C.; Chae, K. S.; Chang, Y.; Lee, G. H. Paramagnetic Ultrasmall Gadolinium Oxide Nanoparticles as Advanced T_1 MRI Contrast Agent: Account for Large Longitudinal Relaxivity, Optimal Particle Diameter, and *In Vivo* T1MR Images. *ACS Nano* **2009**, *3*, 3663–3669.
52. Ahrén, M.; Selegård, L.; Klasson, A.; Söderlind, F.; Abrikossova, N.; Skoglund, C.; Bengtsson, T.; Engström, M.; Käll, P.-O.; Uvdal, K. Synthesis and Characterization of PEGylated Gd_2O_3 Nanoparticles for MRI Contrast Enhancement. *Langmuir* **2010**, *26*, 5753–5762.
53. Shi, Z.; Neoh, K. G.; Kang, E. T.; Shuter, B.; Wang, S. C. Bifunctional Eu^{3+}-Doped Gd_2O_3 Nanoparticles as a Luminescent and T_1 Contrast Agent for Stem Cell Labeling. *Contrast Media Mol. Imaging* **2010**, *5*, 105–111.
54. Huang, C.-C.; Liu, T.-Y.; Su, C.-H.; Lo, Y.-W.; Chen, J.-H.; Yeh, C.-S. Superparamagnetic Hollow and Paramagnetic Porous Gd_2O_3 Particles. *Chem. Mater.* **2008**, *20*, 3840–3848.
55. Bridot, J.; Faure, A.; Laurent, S.; Rivière, C.; Billotey, C.; Hiba, B.; Janier, M.; Josserand, V.; Coll, J.; Vander Elst, L.; *et al.* Hybrid Gadolinium Oxide Nanoparticles: Multimodal Contrast Agents for *In Vivo* Imaging. *J. Am. Chem. Soc.* **2007**, *129*, 5076–5084.
56. McDonald, M. A.; Watkin, K. L. Investigations into the Physicochemical Properties of Dextran Small Particulate Gadolinium Oxide Nanoparticles. *Acad. Radiol.* **2006**, *13*, 421–427.
57. Fortin, M. A.; Petoral, R. M., Jr.; Söderlind, F.; Klasson, A.; Engström, M.; Veres, T.; Käll, P.-O.; Uvdal, K. Polyethylene Glycol-Covered Ultra-Small Gd_2O_3 Nanoparticles for Positive Contrast at 1.5 T Magnetic Resonance Clinical Scanning. *Nanotechnology* **2007**, *18*, 395501(1–9).
58. Wang, Y.; Hussain, S.; Krestin, G. Superparamagnetic Iron Oxide Contrast Agents: Physicochemical Characteristics and Applications in MR Imaging. *Eur. Radiol.* **2001**, *11*, 2319–2331.
59. Josephson, L.; Tung, C.; Moore, A.; Weissleder, R. High-Efficiency Intracellular Magnetic Labeling with Novel Superparamagnetic-Tat Peptide Conjugates. *Bioconjugate Chem.* **1999**, *10*, 186–191.
60. Jun, Y.; Huh, Y.; Choi, J.; Lee, J.; Song, H.; Kim, K.; Yoon, S.; Kim, K.; Shin, J.; Suh, J.; *et al.* Nanoscale Size Effect of Magnetic Nanocrystals and Their Utilization for Cancer Diagnosis *via* Magnetic Resonance Imaging. *J. Am. Chem. Soc.* **2005**, *127*, 5732–5733.
61. Jun, Y.; Seo, J.; Cheon, J. Nanoscaling Laws of Magnetic Nanoparticles and Their Applicabilities in Biomedical Sciences. *Acc. Chem. Res.* **2008**, *41*, 179–189.
62. Lou, X. W.; Archer, L. A. A General Route to Nonspherical Anatase TiO_2 Hollow Colloids and Magnetic Multifunctional Particles. *Adv. Mater.* **2008**, *20*, 1853–1858.
63. Chen, J. S.; Chen, C.; Liu, J.; Xu, R.; Qiao, S. Z.; Lou, X. W. Ellipsoidal Hollow Nanostructures Assembled from Anatase TiO_2 Nanosheets as a Magnetically Separable Photocatalyst. *Chem. Commun.* **2011**, *47*, 2631–2633.